Journal of Water Process Engineering 91 (2026) 110419

Contents lists available at ScienceDirect

Journal of Water Process Engineering

journal homepage: www.elsevier.com/locate/jwpe

Construction of high-temperature resistant graphene oxide framework membranes via interlayer chemical microenvironment engineering for enhanced desalination of oilfield produced water

Jincheng Huang, Hui Xu, Xin Lan, Hong Qi *

College of Chemical Engineering, Nanjing Tech University, Nanjing, 210009, China

ARTICLE INFO

Editor: Mingmei Ding

Keywords:
GO membrane
Oilfield produced water
Desalination
High-temperature resistance

ABSTRACT

Graphene oxide (GO) membranes were first explored for the advanced desalination of pretreated oilfield produced water. Herein, ethylenediamine (EDA) and poly(diallyldimethylammonium chloride) (PDDA) were co-intercalated into the GO membrane interlayers, where EDA mainly served as a structural crosslinker and PDDA regulated the interlayer charge density and hydrophilic microenvironment. This not only enhanced the membrane hydrophilicity and accelerated the selective transport of water molecules but also improved separation performance and high-temperature resistance. The prepared PDDA-GO-EDA-2/Al_2O_3 membrane exhibits exceptionally high water permeance, reaching 14.3 $l \cdot m^{-2} \cdot h^{-1} \cdot bar^{-1}$. It demonstrates rejection rates of 95.0% and 96.0% for $CaCl_2$ and $MgCl_2$, respectively. Notably, after 680 hour immersion in pure water, the PDDA-GO-EDA/Al_2O_3 membrane retained high separation performance. In the simulated treatment of high-temperature and high-salinity produced water, the rejection rates of $CaCl_2$ and $MgCl_2$ remained above 90%. In summary, our work provides an effective strategy for fabricating high temperature resistant GO membranes with superior separation performance.

1. Introduction

Large volumes of produced water are generated during oil and gas production, containing complex organic and inorganic pollutants that pose significant environmental risks [1,2]. Global freshwater scarcity and environmental pressures are driving demand for the resource recovery of produced water, yet existing technologies are hindered by intrinsically low processing efficiency, prohibitively high operational costs, and the potential for secondary environmental contamination [3–5]. In addition, conventional treatment methods often prove ineffective in meeting the stringent regulatory requirements for reuse or discharge of the produced water, particularly concerning the removal of high salinity and recalcitrant pollutants [6,7].

Compared with traditional purification techniques (such as chemical precipitation [8], chemical oxidation [9], adsorption [10], and thermal distillation [11]), membrane separation technology holds significant promise for practical implementation, owing to its inherent advantages, including a compact physical footprint, low specific energy demand, high separation selectivity and permeance, and operation without the need for chemical additives or reactive reagents [12–14].

Graphene oxide (GO) has emerged as a material of significant interest due to its remarkable mechanical strength and outstanding physicochemical properties [15,16]. Stacked GO membranes possess nanoscale and sub-nanoscale mass-transfer channels, which enable high solute rejection. However, their low water permeance often severely limits practical application [17,18].

A promising strategy to address this challenge involves tailoring the interlayer structure and chemical microenvironment of GO membranes. Zhang et al. [19] put forward an interlayer molecular bridge strategy. By rationally constructing and modulating these molecular bridges, the fabricated GO-based membranes not only resist swelling in aqueous environments but also exhibit outstanding stability under demanding operational conditions. Furthermore, Dai et al. [20] introduced sodium polystyrene sulfonate (PSSNa) into the GO membrane interlayers. This dual modification not only stabilized the stacked GO laminates but also established a high-density hydrophilic microenvironment within the interlayers, thereby promoting selective water permeation. Liu et al. [21] introduced diverse polyelectrolytes between MXene membrane layers to modulate the physicochemical properties of the interlayer structure, and achieved outstanding pervaporation dehydration of

* Corresponding author.
E-mail address: hqi@njtech.edu.cn (H. Qi).

https://doi.org/10.1016/j.jwpe.2026.110419
Received 7 April 2026; Received in revised form 12 June 2026; Accepted 15 June 2026
Available online 30 June 2026
2214-7144/© 2026 Elsevier Ltd. All rights are reserved, including those for text and data mining, AI training, and similar technologies.

isopropanol/water mixtures. Liu et al. [22] reported an atomic-scale "chemical microenvironment engineering" strategy, which enabled precise customization of COF membrane edge structures. "Chemical microenvironment engineering" strategy enhances improves the water-affinity of confined nanochannels, creating low-resistance water transport pathways that improve separation efficiency. Wu et al. [23] developed positively charged MXene membranes by intercalating poly (diallyl dimethyl ammonium chloride) (PDDA) into the MXene interlayers. The incorporation of PDDA enhanced the Donnan exclusion effect and significantly boosted Li^+/Mg^{2+} selectivity.

Therefore, a critical approach to enhancing GO membrane separation efficiency is improving the stability of the GO membrane lamellar structure while simultaneously establishing distinct chemical environments and specialized functional structures between the layers.

To address the intrinsic drawbacks of GO membranes in produced water treatment, including interlayer swelling, insufficient structural stability, and the difficulty in simultaneously achieving high permeability and selectivity, an interlayer chemical microenvironment engineering strategy was proposed in this work. Ethylenediamine (EDA) and poly(diallyldimethylammonium chloride) (PDDA) were co-intercalated into the GO galleries as dual-functional regulators. Specifically, EDA was used as an interlayer crosslinking agent to reinforce the GO lamellar structure and suppress swelling, while PDDA was introduced as a cationic hydrophilic polymer to regulate the interlayer charge density and hydrophilic microenvironment. Through this design, two-dimensional confined channels integrating network-like sieving structures with hydrophilic chemical microdomains were constructed, and the lamellar structure of the GO membrane was expected to be reinforced, thereby suppressing interlayer swelling and structural deterioration under aqueous and high-temperature conditions. Meanwhile, by tailoring the interlayer charge environment and transport microstructure, the synergistic effects of Donnan exclusion and interlayer sieving were expected to be strengthened, enabling the integration of fast water transport with highly selective ion separation. On this basis, this study aims to develop a GO-based composite nanofiltration membrane for the deep desalination of pretreated high-temperature and high-salinity oilfield produced water, with enhanced permeability, improved salt rejection, and robust thermal stability. The fabrication route is illustrated in Fig. 1.

2. Experimental

2.1. Materials

Al_2O_3 tubular ceramic substrates (porosity: ~35%; inner diameters: 8 mm; outer diameters: 12 mm; length: 12 cm; average pore size: 20 nm) and deionized water (conductivity: 5 $\mu S \cdot cm^{-1}$) were provided by Nanjing Hongyi Ceramic Nanofiltration Membrane Co., Ltd. The GO dispersion (concentration: 1 $mg \cdot ml^{-1}$, flake sizes: 0.5–5 μm) was obtained from Nanjing XF Nanomaterials Technology. Tris(hydroxymethyl)aminomethane (Tris, $C_4H_{11}NO_3$, 121.14 Da), Dopamine hydrochloride ($C_8H_{12}ClNO_2$, 189.64 Da), and poly (diallyl dimethyl ammonium chloride) (PDDA, Mw 200 k–350 k) were procured from Shanghai Aladdin Bio-Chem Technology Co., Ltd. Ethylenediamine (EDA, $C_2H_8N_2$, 60.10 Da), Hydrochloric acid (HCl, 36 wt%), and inorganic salts (NaCl, $CaCl_2$, $MgCl_2$) were obtained from Shanghai Experimental Reagent Co., Ltd.

2.2. Preparation of PDA-Al_2O_3 substrate

PDA-Al_2O_3 substrate was prepared by immersing the tubular Al_2O_3 ceramic support in a dopamine-containing Tris-HCl aqueous solution to allow the self-polymerization and deposition of polydopamine on the substrate surface. After rinsing with deionized water and drying, the obtained membrane was denoted as PDA-Al_2O_3. Detailed preparation conditions are provided in the Supporting Information.

2.3. Preparation of GO-based membranes

First, the GO dispersion was diluted to a concentration of 0.001 $mg \cdot ml^{-1}$. Subsequently, 200 ml of the GO dispersion were measured after 5 min ultrasonication. Different amounts of EDA (0.5, 1.0, and 1.5 mmol) were then added into the GO dispersion, followed by stirring in an 80 °C constant-temperature water bath for 60 min to obtain the GO-EDA membrane-forming solution. The detailed membrane separation

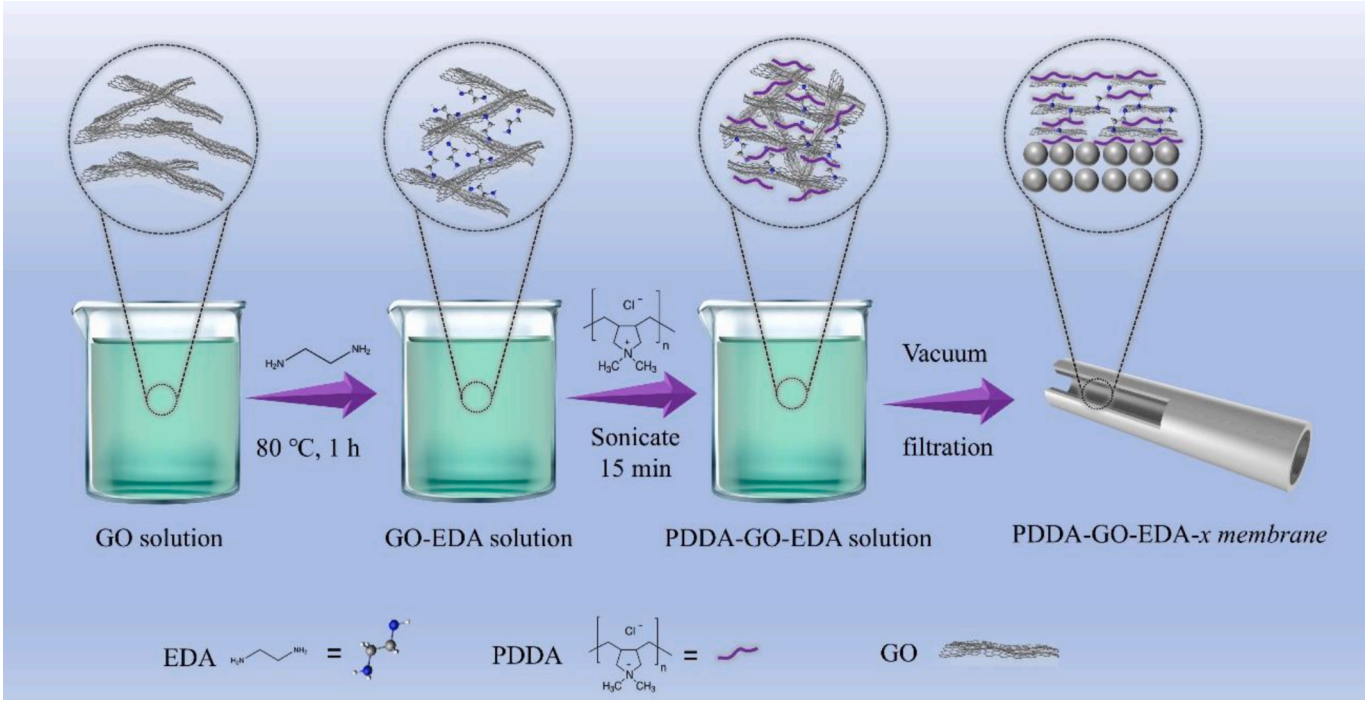


Fig. 1. Fabrication process of the PDDA-GO-EDA-x/Al_2O_3 membranes.

performances under different EDA dosages are provided in Fig. S1. Based on the comprehensive evaluation of water permeance and salt rejection, 1 millimole EDA was selected for the following membrane fabrication unless otherwise specified. Finally, coating was performed using the coating apparatus (Fig. S2), followed by drying overnight at 40 °C to produce the GO-EDA membrane (abbreviated as GE membrane).

A defined volume of PDDA solution was added to the GO-EDA membrane-forming solution prepared in Step 1, followed by ultrasonication for 15 min to obtain poly (diallyl dimethyl ammonium chloride)-graphene oxide-ethylenediamine membrane-forming solution. PDDA-GO-EDA/Al_2O_3 membranes were obtained via identical coating and drying procedures. Theoretical mass ratios of GO to PDDA were set at 1:200, 1:350, and 1:500, with the composite films labelled PDDA-GO-EDA-1/Al_2O_3 (abbreviated as PGE-1 membrane), PDDA-GO-EDA-2/Al_2O_3 (abbreviated as PGE-2 membrane), and PDDA-GO-EDA-3/Al_2O_3 (abbreviated as PGE-3 membrane), respectively.

The PDDA-GO membrane-forming solution was prepared by adding a measured amount of PDDA to 200 ml of GO dispersion, followed by sonication for 15 min. The PDDA-GO/Al_2O_3 membrane, denoted as PG membrane, was then fabricated using the same coating and drying procedures.

2.4. Characterizations

Fourier transform infrared spectroscopy (FT-IR, Nicolet 8700) and X-ray photoelectron spectroscopy (XPS, ESCALAB 250) were performed to investigate the chemical composition of the membranes. X-ray diffraction (XRD, Mini Flex 600) was performed at 40 kV and 15 mA with Cu-Kα radiation (λ = 0.154 nm) to determine the interlayer spacing of the GO-based membranes. The microscopic morphology of GO-based membranes was characterized by scanning electron microscopy (SEM, S-4800). Raman spectroscopy was performed using a DXR2xi Raman imaging microscope (Thermo Fisher Scientific, USA) to characterize the structural features of the original GO nanosheets. The thickness of GO nanosheets was studied by an atomic force microscope (AFM, XE-100, Park SYSTEMS, Korea). The zeta potentials of the membrane-forming dispersions were measured using a zeta-sizer instrument (DLS, ZS-90). Water contact angles (WCA) of the GO-based membranes were obtained using a contact angle tester (Drop Meter A-100P). Determination of the conductivity of ions in salt solutions was performed using a conductivity meter (DDS-307).

2.5. Separation performance of GO-based membranes

GO-based membranes were tested for their pure water permeance, salt rejection, long-term desalination and high-temperature desalination performance using the apparatus as described in Fig. S3. The membrane was tested at a constant transmembrane pressure difference (0.5 MPa), crossflow velocity (1.3 $m{\cdot}s^{-1}$), and temperature (25 °C or 85 °C). To test the pure water permeance of GO-based membrane, permeate was collected every 5 min over a continuous 4-h period. The pure water permeance rate (J) was calculated using Eq. (1).

For the salt rejection testing involving three salts (1 mM $CaCl_2$, $MgCl_2$, NaCl), permeate was collected at five-minute intervals following 40 min of system stabilization, yielding a total of four samples. Conductivity was measured with a conductivity meter, and salt rejection rates (R) were calculated using Eq. (2). The GO-based membrane was immersed in pure water for 170, 340, 510, and 680 h, respectively. After each immersion period, its retention of the three salts was retested to characterize the desalination stability. For high-temperature testing, the filtration system temperature was elevated to 85 °C. Following a 40-min stabilization period, permeate samples were collected at 10-min intervals.

The pure water permeance J ($l{\cdot}m^{-2}{\cdot}h^{-1}{\cdot}bar^{-1}$) and the salt rejection R are calculated with Eqs. (1) and (2):

$$J = \frac{V}{At\Delta P} \tag{1}$$

where V (L) is the permeate volume, A (m^2) is the effective membrane area, t (h) is the permeation time, and ΔP (bar) is the operating pressure.

$$R = \left(1 - \frac{C_p}{C_f}\right) \times 100\% \tag{2}$$

where C_f and C_p are the feed and permeate salt concentrations, respectively.

3. Results and discussion

3.1. Characterizations of GO nanosheets

GO nanosheets serve as the fundamental building blocks of the membrane. Characterization of the GO nanosheets showed that they possessed large lateral dimensions and atomic-scale thickness, which facilitated their assembly into a lamellar membrane structure. As shown in Fig. 2c, characteristic peaks appeared at approximately 3390, 1730, 1625, and 1052 cm^{-1}, corresponding to hydroxyl, carbonyl, aromatic C═C, and epoxy groups, respectively. These peaks are assigned to the characteristic vibrations of graphene oxide. Raman spectroscopy was further employed to characterize the structural features of the original GO nanosheets, and the corresponding result is provided in Fig. S4. Two typical peaks appear at approximately 1350 and 1590 cm^{-1}, corresponding to the D band and G band of GO, respectively. The presence of these two characteristic bands further confirms the defect-containing graphitic framework of the GO nanosheets, supporting their use as building blocks for lamellar membrane construction.

3.2. Characterizations of PDA-Al_2O_3 substrate

Self-supporting GO membranes are challenging to deploy in practical applications, underscoring the need to deposit them onto ceramic membranes with their inherent advantages. Visual inspection (Fig. 3a, b) revealed a clear color change after PDA modification, indicating the successful deposition of a PDA coating formed via dopamine self-polymerization on the ceramic substrate surface [24]. In addition, the surface morphology of the substrate became slightly rougher after PDA modification, further suggesting the formation of a PDA layer. To evaluate the impact of PDA modification on the substrate, both pristine and PDA-modified ceramic substrates were tested for permeability and salt rejection. The results (Fig. S5 and Table S1) show that PDA modification caused only a minor reduction in permeability (from 268.9 to 242.4 $l{\cdot}m^{-2}{\cdot}h^{-1}{\cdot}bar^{-1}$) and had no influence on salt rejection, as evidenced by zero rejection of all three salts.

3.3. Characterizations of GO-based membranes

For separation membranes, an intact membrane laminar structure is crucial. The surfaces of the five prepared GO-based membranes exhibit no defects (Fig. 4a–e), thereby providing the necessary conditions for achieving superior separation performance. The layer thicknesses of the five GO-based membranes were 55, 94, 184, 204, and 236 nm, respectively (Fig. 4f–j). We further characterized the PGE-2 membrane surface by SEM-EDS mapping, which revealed the spatial distribution of Al, C, N, O, and Cl elements on the membrane surface (Fig. 4k–o).

The chemical properties of the five GO-based membranes were further analyzed by FT-IR and XPS. The pristine GO membrane displayed characteristic peaks at ~3390, ~1730, ~1625, and ~ 1052 cm^{-1} (Fig. 5a), corresponding to hydroxyl, carbonyl, aromatic, and epoxy groups, respectively, consistent with the previous report [25].

Apart from the bands derived from GO, new characteristic peaks were observed at ~1580 and ~ 1475 cm^{-1}, corresponding to N—H and

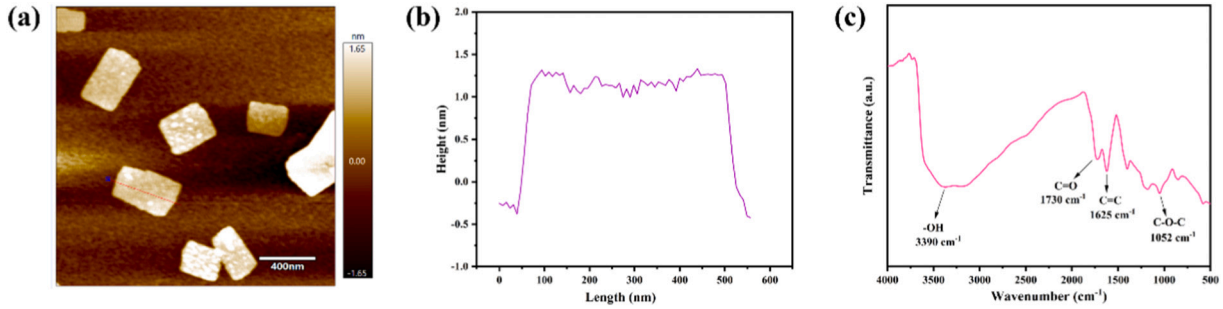


Fig. 2. Characterizations of GO nanosheets. (a) AFM image, (b) corresponding height, and (c) FTIR spectrum.

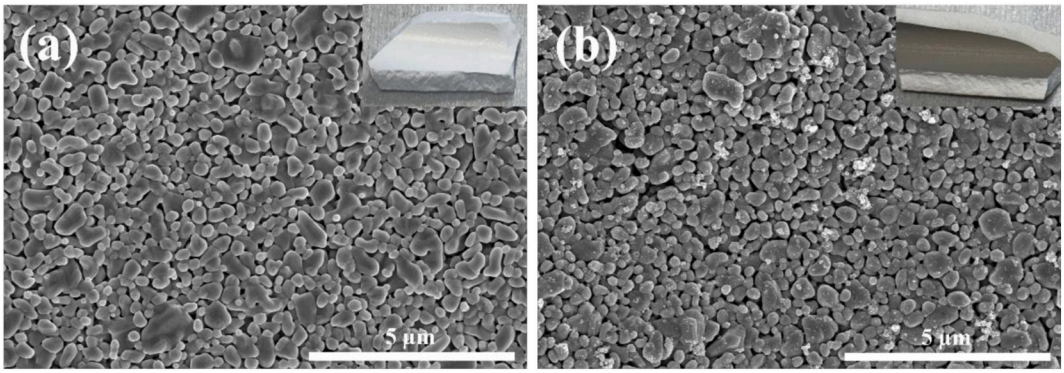


Fig. 3. SEM images of (a) pristine Al_2O_3 substrate and (b) PDA-modified Al_2O_3 substrate surface.

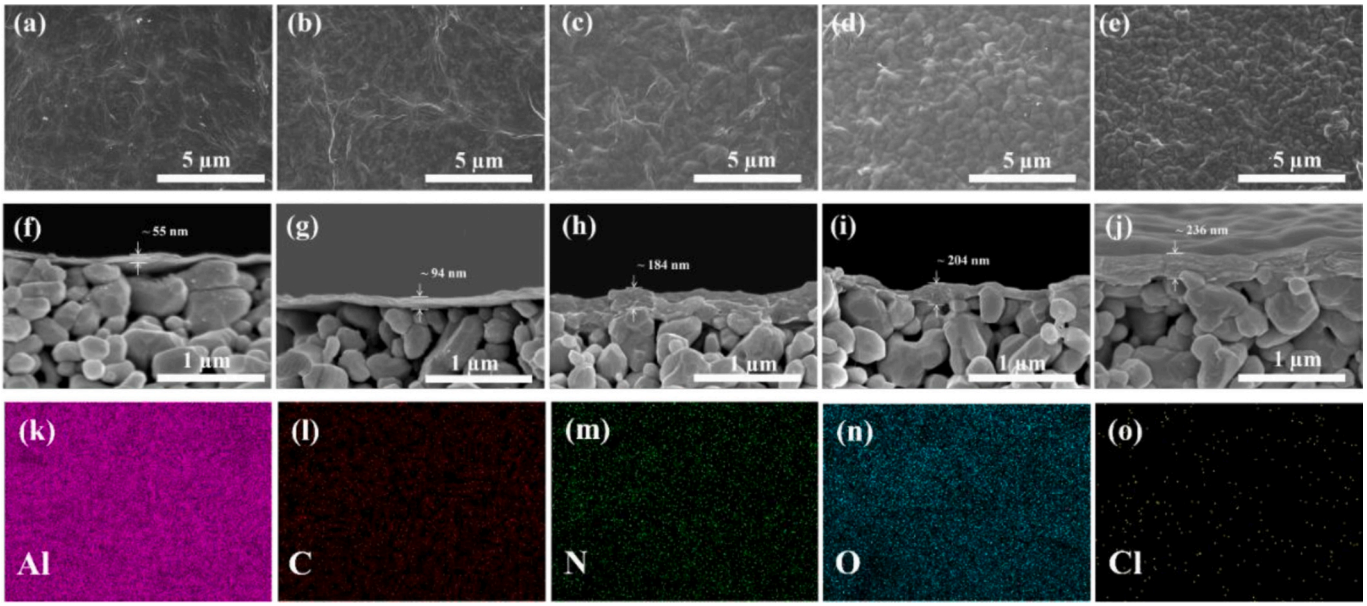


Fig. 4. SEM images of GO (a, f), GE (b, g), PGE-1 (c, h), PGE-2 (d, i), and PGE-3 (e, j) membranes; (k–o) SEM-EDS elemental mappings of the PGE-2 membrane surface.

C-N/N^+-R_4 respectively [19,26]. These results provide evidence that the amine monomers undergo chemical reactions with the oxygen-containing groups on GO nanosheets. These reactions establish covalent crosslinks via two distinct mechanisms: condensation and nucleophilic addition [27].

Additionally, in contrast to the pristine GO membrane, new N 1 s peaks at ~400 eV were observed for the other four membranes (Fig. 5b), confirming the presence of nitrogen-containing groups [28]. In contrast to the GO and GE membranes, the PGE membranes exhibited an additional Cl 2p peak at ~198 eV [29]. Deconvolution of the N 1 s spectrum for the PGE membranes (Fig. 5c–e) revealed two peaks at ~402.0 eV and ~ 399.0 eV. The higher binding energy peak is attributed to the positively charged quaternary ammonium group, while the lower binding energy peak corresponds to the uncharged amine or amide group. Combined with infrared spectroscopy analysis, surface element distribution mapping, and detailed N 1 s spectrum analysis, these results provide strong evidence for the successful incorporation of EDA and PDDA into the GO membrane, thereby regulating the interlayer

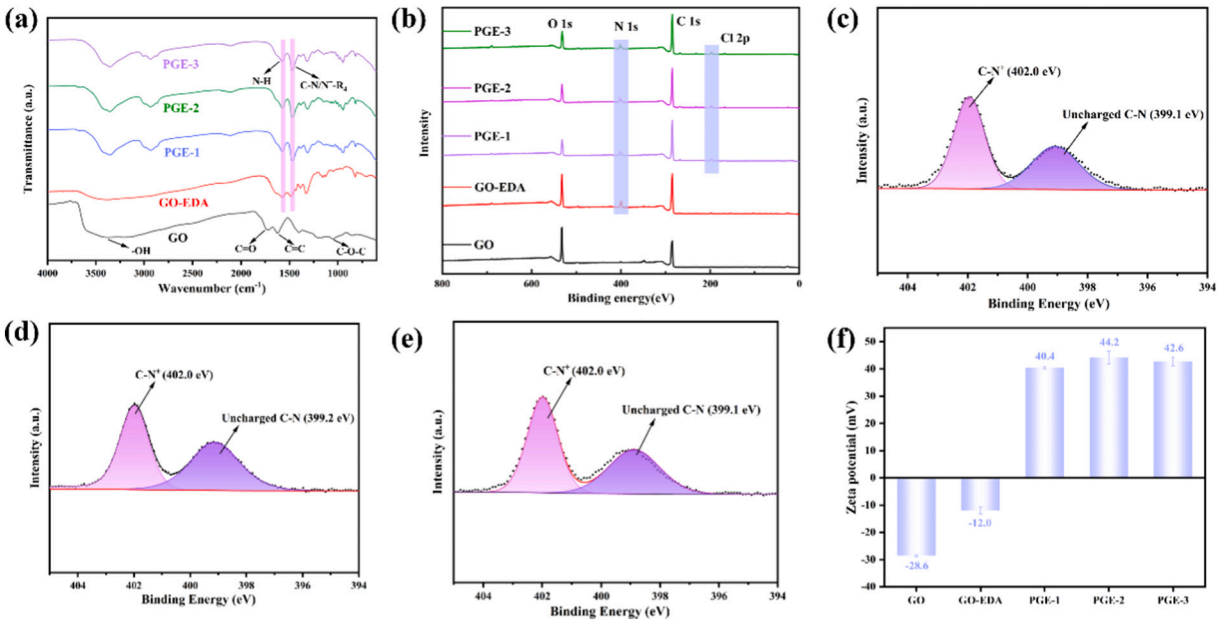


Fig. 5. Chemical characterization of the five GO membranes. (a) ATR-FTIR spectra, (b) XPS survey spectra, (c–e) high-resolution N 1s spectra of PGE-1, PGE-2, and PGE-3 membrane, and (f) zeta potential.

chemical environment and transport channels.

Given the critical role of the Donnan exclusion effect in nanofiltration performance, we measured the zeta potential of the five membrane-forming dispersions (Fig. 5f). The addition of EDA resulted in a decrease in absolute zeta potential, while subsequent incorporation of PDDA led to a marked increase. This trend reflects the underlying chemistry: EDA consumes oxygenated groups on GO via covalent reactions, reducing negative charge density; conversely, PDDA contributes quaternary ammonium groups with permanent positive charges, enhancing the net positive charge. The pH-dependent zeta potentials of GO, GO-EDA, and PGE-2 membrane-forming dispersions are provided in Fig. S6. The results show that GO and GO-EDA dispersions remained negatively charged over most of the tested pH range, while the PGE-2 dispersion exhibited positive zeta potentials due to the quaternary ammonium groups of PDDA. These results further confirm the charge-regulation effect of PDDA in the GO-based system. The excellent dispersibility of all five membrane-forming solutions facilitates the homogeneous assembly of GO nanosheets onto tubular ceramic substrates, ultimately producing membranes with well-defined lamellar structures.

Surface hydrophilicity plays a crucial role in the performance of separation membranes, as it governs water permeation behavior by promoting favorable interactions between the membrane surface and water molecules. To assess this property, we measured the water contact angle for each of the five fabricated membranes. A consistent reduction in contact angles across the series indicates a systematic improvement in surface wettability (Fig. 6d). This enhancement can be attributed to the incorporation of hydrophilic diamine and quaternary ammonium groups, which create hydrophilic domains on the membrane surface, promoting stronger interactions with water molecules.

Additionally, the diffraction peak at 10.93° was observed for the pristine GO membrane in the XRD patterns of the dry GO-based membranes (Fig. 6a), corresponding to an interlayer spacing of 0.805 nm, in agreement with the literature [30]. For four other membranes, the diffraction peaks shifted toward lower angles, indicating progressively larger interlayer spacings. The swelling resistance of the five GO membranes in aqueous environments was evaluated. After thorough wetting in pure water, the diffraction peaks of the pristine GO membrane shifted toward lower angles, indicating an increase in interlayer spacing to 1.282 nm (Fig. 6b–c). The increased interlayer spacing under wet conditions is due to water intercalation, which disrupts inter-nanosheet hydrogen bonds and π-π interactions, causing the GO laminates to swell. The dry/wet XRD results provide direct evidence for the interlayer regulation and swelling resistance of the EDA/PDDA-modified GO membranes.

For both GE and PGE membranes, the relative change in interlayer spacing was comparatively smaller, attributable to the following three synergistic factors: (i) the formation of covalent C—N bonds; (ii) electrostatic interactions between the quaternary ammonium groups of

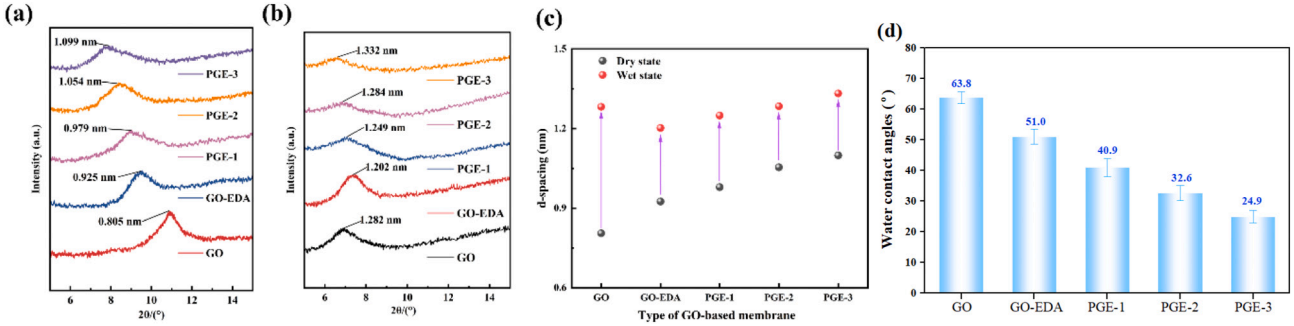


Fig. 6. XRD patterns of the five GO membranes in the (a) dry and (b) wet states, (c) corresponding d-spacing values under dry and wet states, (d) water contact angles of the five GO membranes.

PDDA and oxygen-containing functional groups on GO nanosheets; and (iii) the hierarchical network architecture arising from the near-perpendicular orientation of C—N covalent bonds [31] and the near-parallel alignment of PDDA polymer chains [23].

The enhanced structural stability of the GO membrane is attributed to the effective mitigation of its swelling tendency, which preserves a more robust two-dimensional lamellar structure relative to the pristine GO membrane.

3.4. Permeability of GO-based membranes

First, we conducted a continuous 4-hour test to determine the water permeance of the five GO membranes. The water permeabilities of the five GO membranes were 1.2, 2.6, 18.6, 14.3, and 9.1 $l \cdot m^{-2} \cdot h^{-1} \cdot bar^{-1}$ (Fig. 7a–b). The intercalation and crosslinking of EDA increased the d-spacing of the GE membrane, resulting in enhanced permeability.

Concurrently, with the increase of the PDDA doping content, the permeability of the PGE membranes improved by 15.5-fold, 11.9-fold, and 7.6-fold relative to the pristine GO membrane, albeit with a diminishing enhancement trend. This behavior can be attributed to the formation of a high-density network of hydrophilic domains within the GO interlayers, which creates additional pathways for water transport. The permanently positively charged quaternary ammonium groups in PDDA exhibit a strong affinity for water molecules, enabling the adsorbed water to maintain high mobility and facilitating rapid water transport along the PDDA chains confined within the nanochannels.

Consequently, the permeability of the PGE series membranes with different contents of PDDA is significantly enhanced. However, compared to the PDDA-GO-EDA-1 membrane, the PDDA-GO-EDA-2 and PDDA-GO-EDA-3 membranes contain more intercalated PDDA between interlayers, forming increasingly complex reticular structures. This results in tortuous and prolonged water transport pathways, along with progressively thicker membrane layers, thereby increasing the transfer resistance encountered by water molecules. Hence, the permeability enhancement observed in the other two PGE membranes is less pronounced than that observed in the PGE-1 membrane.

3.5. Separation performance of GO-based membranes

Due to the presence of significant amounts of Ca^{2+}, Mg^{2+}, Na^{+}, Cl^{-}, and other ions in produced water from offshore oilfields, we primarily conducted desalination tests on three inorganic salts: $CaCl_2$, $MgCl_2$, and NaCl. The rejection order of the three salts by GO and GE membranes follows $R(CaCl_2) > R(NaCl) > R(MgCl_2)$ (Fig. 8a, b, c), which can be attributed to the combined effects of Donnan exclusion, size sieving, ion hydration, and ion-specific charge-screening behavior. For the GE membrane, Mg^{2+} may more effectively screen the membrane charge and weaken the electrostatic exclusion of Cl^{-}, leading to a lower apparent rejection of $MgCl_2$ than NaCl [32]. The rejection rates of the PGE membranes for $CaCl_2$, $MgCl_2$, and NaCl were as follows: 89%, 88%, and 70% for PGE-1; 95%, 96%, and 70% for PGE-2; 92%, 90%, and 73% for PGE-3. The PGE series membranes demonstrated significantly higher retention of all three salts compared to the pristine GO membrane. This improvement can be mainly attributed to the incorporation of positively charged PDDA into the GO interlayers, which enhances the Donnan exclusion effect. Meanwhile, EDA-mediated interlayer connections may help stabilize the confined GO lamellar structure, while PDDA polymer chains further regulate the interlayer transport pathways and strengthen the combined effects of interlayer sieving and electrostatic exclusion. In contrast, the PGE-1 membrane contains a lower PDDA content, resulting in weaker Donnan and size-exclusion effects. Consequently, the salt rejection rates of PDDA-GO-EDA-1 for the three salts are slightly lower than those of the other two PGE membranes. Although the PDDA-GO-EDA-2 and PDDA-GO-EDA-3 membranes exhibited comparable salt rejection performance, the PDDA-GO-EDA-2 membrane demonstrated superior water permeance, thus rendering it the most promising GO-based membrane for practical applications. The potential separation mechanism of the PDDA-GO-EDA membrane is proposed (Fig. 8d). In addition, the effects of operating pressure and crossflow velocity on the separation performance of the optimized PGE-2 membrane were further investigated. As shown in Fig. S7, increasing the operating pressure enhanced the water flux and slightly improved the salt rejection, while increasing the crossflow velocity improved the membrane permeance and salt rejection by mitigating concentration polarization and enhancing mass transfer near the membrane surface. These results indicate that the PGE-2 membrane has good operational adaptability under different operating conditions. Additional salt rejection tests using representative salts with different valences and ionic strengths were further conducted for the optimized PGE-2 membrane, and the corresponding results are provided in Fig. S8 and Table S2. These results further support that the salt rejection behavior of the PGE-2 membrane is associated with the combined effects of size sieving, Donnan exclusion, ion hydration, charge screening, and the positively charged/hydrophilic interlayer microenvironment introduced by PDDA.

3.6. Stability of GO-based membranes

Membrane stability is a key factor in determining its suitability for practical applications. To assess this, we investigated the stability of five GO membranes in aqueous solutions. The results (Figs. 9 and S9) reveal that the rejection performance of the GO, GE, and PGE-2 membranes toward the three salt solutions remained relatively stable, with only minor fluctuations and no significant decline after prolonged immersion. Specifically, the PGE-2 membrane consistently maintained a rejection rate of ~90% for both $CaCl_2$ and $MgCl_2$. By contrast, although the PGE-1 and PGE-3 membranes exhibited increased permeability,

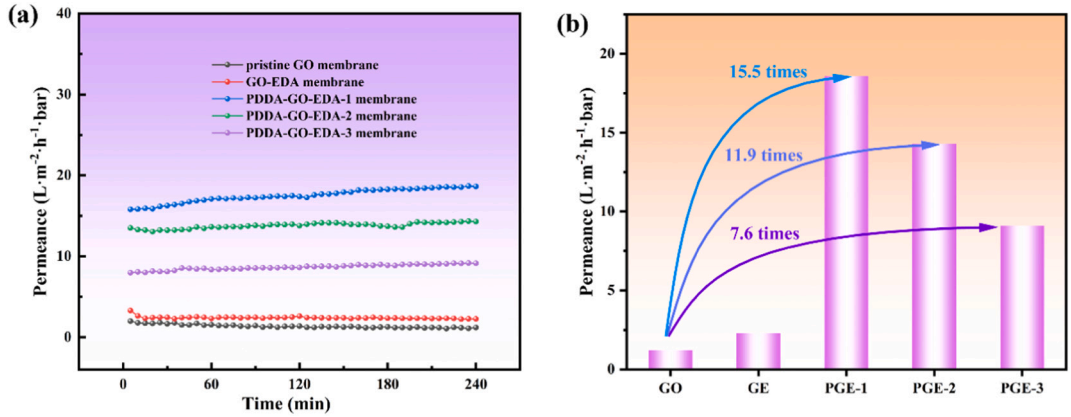


Fig. 7. Water permeance of the five GO membranes.

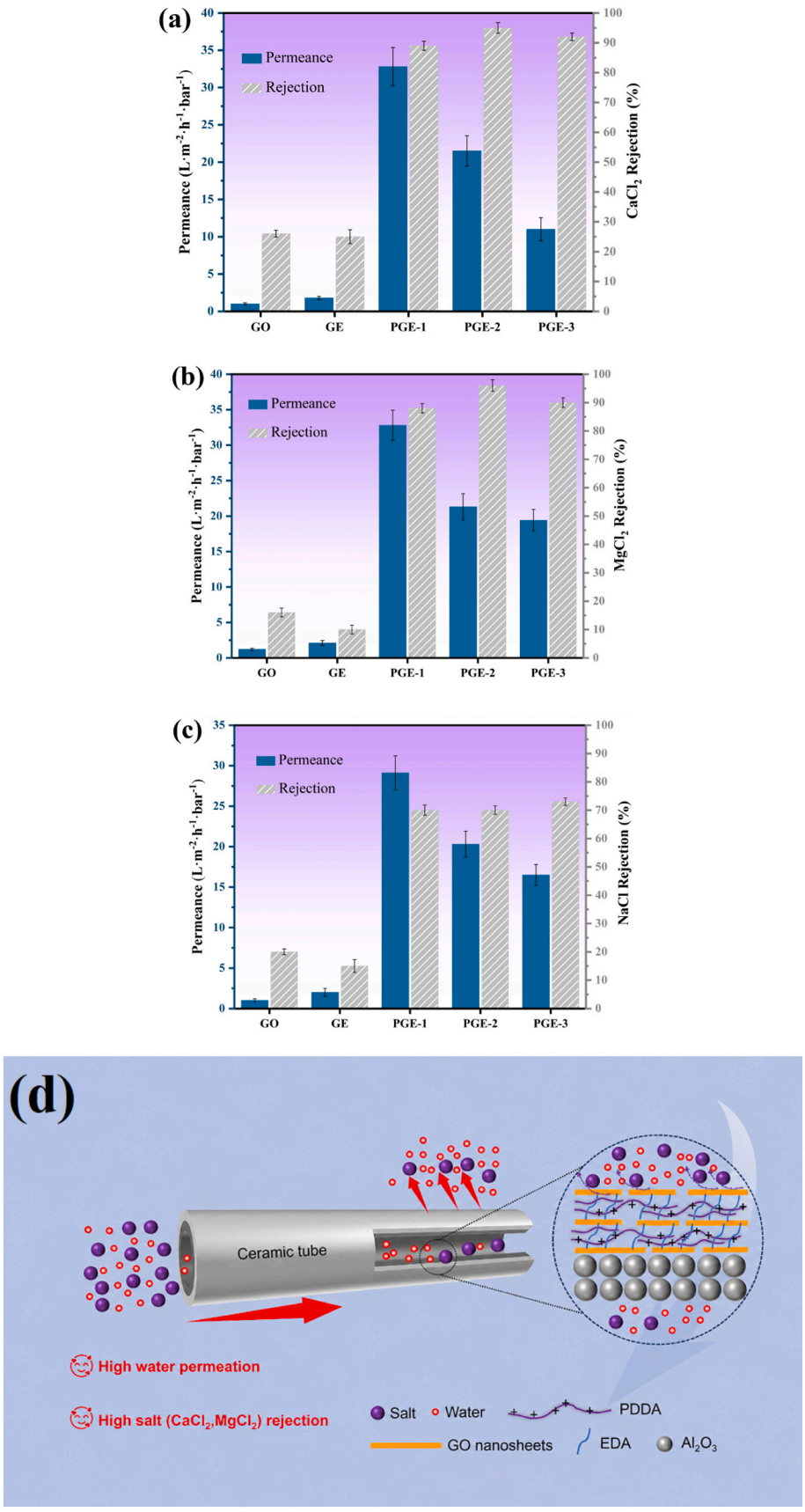


Fig. 8. Nanofiltration performance of (a) PGE-1, (b) PGE-2, (c) PGE-3 membrane, (d) potential separation mechanism of the PDDA-GO-EDA-x membrane.

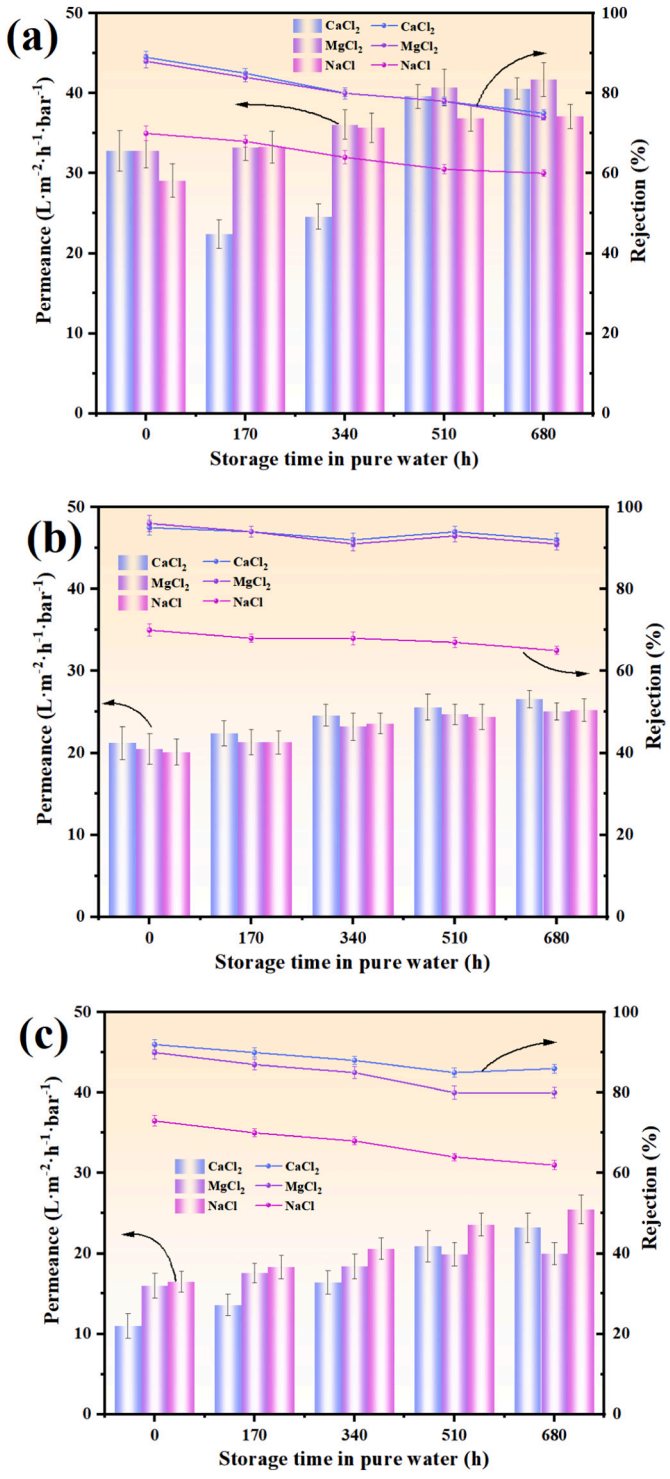


Fig. 9. Nanofiltration performance stability of (a) PGE-1, (b) PGE-2, and (c) PGE-3 membrane.

their rejection rates decreased. This indicates that the PGE-2 membrane exhibits a combination of exceptional stability and high nanofiltration performance in aqueous solutions.

3.7. Synergistic mechanism of EDA and PDDA

We investigated the synergistic effect between EDA and PDDA by focusing on the PGE-2 membrane, which demonstrated the optimal nanofiltration performance. For comparison, we prepared PDDA-GO membranes using the same coating and drying methods after uniformly mixing PDDA with GO. The PDDA-GO membrane exhibited a 3.1-fold enhancement in permeability and increased rejection rates (53% for $CaCl_2$, 70% for $MgCl_2$, and 13% for NaCl) compared to the GO-EDA membrane (Fig. 10a–b and Table S3). However, the enhancements observed in this instance were considerably less substantial compared to those evident in the PGE-2 membrane. The superior performance of the PGE-2 membrane comes from its unique interlayer architecture. The combination of hydrophilic EDA and highly hydrophilic PDDA endows the PGE-2 membrane with greater overall hydrophilicity compared to the singly crosslinked GO-EDA and PDDA-GO membranes, thereby enhancing its water permeance. Furthermore, the PGE-2 membrane possesses a more intricate interlayer network. Specifically, EDA molecules are likely to connect adjacent GO nanosheets, while the long and flexible PDDA chains may regulate the interlayer transport pathways within the GO galleries.

Based on the FT-IR, XPS, XRD, and separation results, we propose that EDA-mediated interlayer connections and PDDA-assisted polymer-chain regulation jointly contribute to the formation of a stable and selective network-like transport structure within the GO interlayers. This synergistic interlayer structure may enhance the salt selectivity of the PGE-2 membrane and account for its improved rejection performance, as schematically illustrated in Fig. 10c.

3.8. Temperature resistance of the PGE-2 membrane

Oilfield produced water treatment is commonly carried out under elevated temperatures (80–96 °C), with calcium and magnesium concentrations typically ranging from 91 to 874 $mg{\cdot}l^{-1}$ and 11 to 202 $mg{\cdot}l^{-1}$, respectively. In the present experimental setup, $CaCl_2$ and $MgCl_2$ feed solutions were tested at 85 °C, with Ca^{2+} and Mg^{2+} concentrations of 800 $mg{\cdot}l^{-1}$ and 200 $mg{\cdot}l^{-1}$, respectively.

The membrane's performance was evaluated under simulated produced water conditions at a pressure of 5 bar (Fig. 10d and Table S4). After the cross-flow filtration system reached a steady state (40 min of operation), the permeate was immediately collected for conductivity measurement. Compared with operation at ambient temperature, the membrane exhibited a higher permeation flux at elevated temperature, which was mainly attributed to the reduced solution viscosity and enhanced mass transfer. Notably, despite the combined effects of elevated temperature and high ionic strength, the membrane still maintained high rejection rates of 90% for $CaCl_2$ and 91% for $MgCl_2$, with only slight fluctuations, demonstrating excellent structural stability and ion-sieving capability.

Mechanistically, elevated temperature generally enhances polymer chain mobility and increases the interlayer free volume, which may induce thermally driven structural relaxation and weaken size-sieving effects. Meanwhile, high concentrations of divalent ions (Ca^{2+} and Mg^{2+}) can cause charge screening, thereby reducing electrostatic repulsion and potentially lowering ion rejection. However, the negligible decline in rejection observed in this study suggests that the membrane possesses strong resistance to thermal swelling and structural degradation. This can be attributed to the synergistic effect between EDA and PDDA within the GO interlayers. Specifically, EDA acts as a crosslinking agent that restricts excessive interlayer expansion via covalent or hydrogen-bond interactions, while PDDA introduces cationic polymer chains that enhance electrostatic interactions and steric hindrance. These combined effects stabilize the lamellar architecture and suppress pore enlargement under harsh conditions, thereby preserving high separation performance.

In addition to the high-temperature desalination test, a total-recycle filtration experiment was further conducted to evaluate the operational stability of the PGE-2 membrane under elevated-temperature conditions. As shown in Fig. S10, the rejection of $CaCl_2$ and $MgCl_2$ remained stable during the 30 h test, with no obvious continuous decline. This result further demonstrates the thermal adaptability and high-

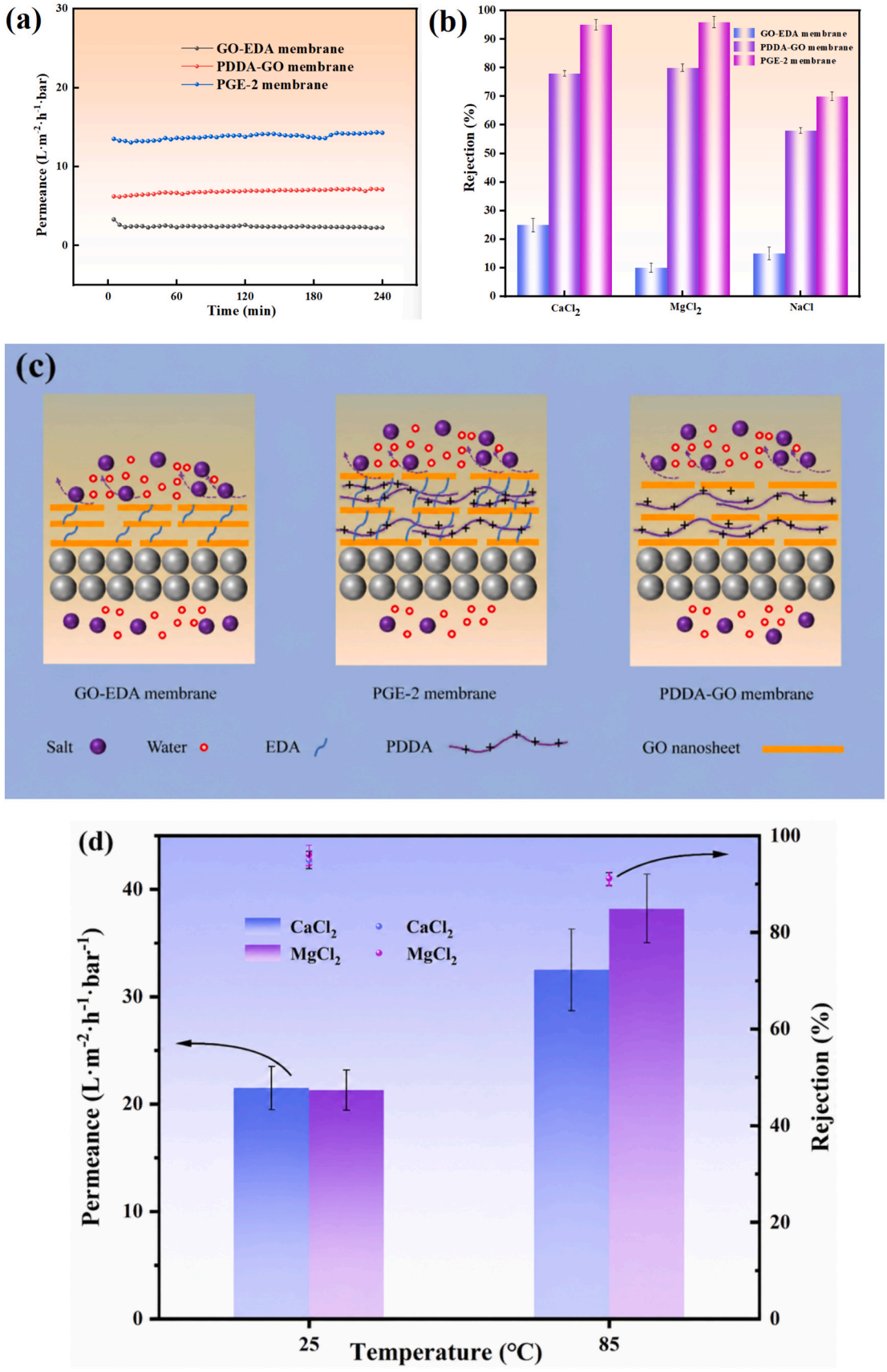


Fig. 10. Synergistic effect of EDA and PDDA and temperature-resistant performance of the PGE-2 membrane: (a) water permeance and (b) salt rejection of GO-EDA, PDDA-GO, and PGE-2 membranes; (c) schematic illustration of the potential synergistic mechanism between EDA and PDDA; and (d) temperature-resistant desalination performance of the PGE-2 membrane.

temperature operational stability of the PGE-2 membrane under laboratory-scale filtration conditions. To further highlight its potential for high-temperature desalination applications, the performance of the present membrane was compared with representative commercial NF/RO membranes, as summarized in Table S5.

4. Conclusion

In this work, a rational interlayer chemical microenvironment engineering strategy was developed for GO-based nanofiltration membranes by co-intercalating EDA and PDDA into the GO galleries. Rather than merely increasing membrane permeability or rejection individually, this dual-functional design simultaneously stabilized the lamellar structure and optimized the interlayer transport environment. Specifically, EDA acted mainly as a molecular bridge to suppress interlayer swelling and reinforce the structural stability of GO laminates, while PDDA introduced hydrophilic and positively charged microdomains that promoted water transport and enhanced Donnan exclusion toward salt ions. The synergistic effect of these two components enabled the construction of stable, hydrated, and ion-selective nanochannels within the GO membrane. The resulting PGE-2 membrane delivers an outstanding permeability of 14.3 $l{\cdot}m^{-2}{\cdot}h^{-1}{\cdot}bar^{-1}$, coupled with excellent divalent salt rejection (95.0% for $CaCl_2$ and 96.0% for $MgCl_2$). More importantly, the membrane maintained stable separation performance after 680 h immersion in water and preserved high divalent-salt rejection under 85 °C simulated produced-water conditions, demonstrating its strong resistance to structural relaxation and thermal degradation. These results indicate that the simultaneous regulation of lamellar stability and interlayer chemical environment is an effective route for overcoming the conventional permeability–selectivity trade-off of GO membranes.

From an application perspective, the present membrane shows promising potential for the advanced desalination of pretreated high-temperature and high-salinity oilfield produced water. Therefore, this ceramic-supported GO membrane may provide a potential route to replace or complement conventional polymeric NF/RO membranes in the advanced desalination step, particularly under high-temperature operating conditions. Nevertheless, further studies are still required to evaluate its antifouling behavior, long-term continuous operation stability, and treatment performance toward real produced water containing oils, organics, and suspended solids.

CRediT authorship contribution statement

Jincheng Huang: Writing – original draft, Visualization, Validation, Methodology, Investigation, Formal analysis, Data curation, Conceptualization. **Hui Xu:** Writing – original draft, Visualization, Investigation, Formal analysis. **Xin Lan:** Visualization, Investigation, Formal analysis. **Hong Qi:** Writing – review & editing, Validation, Supervision, Resources, Project administration, Funding acquisition.

Declaration of competing interest

The authors declare that they have no known competing financial interests or personal relationships that could have appeared to influence the work reported in this paper.

Acknowledgments

This study was supported by the National Natural Science Foundation of China (21490581) and China Petroleum & Chemical Corporation (317008-6).

Appendix A. Supplementary data

Supplementary data to this article can be found online at https://doi.org/10.1016/j.jwpe.2026.110419.

Data availability

Data will be made available on request.

References

[1] C.L. Coonrod, Y.B. Yin, T. Hanna, A.J. Atkinson, P.J.J. Alvarez, T.N. Tekavec, M. A. Reynolds, M.S. Wong, Fit-for-purpose treatment goals for produced waters in shale oil and gas fields, Water Res. 173 (2020) 115467, https://doi.org/10.1016/j.watres.2020.115467.
[2] S. Jamaly, A. Giwa, S.W. Hasan, Recent improvements in oily wastewater treatment: progress, challenges, and future opportunities, J. Environ. Sci. 37 (2015) 15–30, https://doi.org/10.1016/j.jes.2015.04.011.
[3] J.S.B. Souza, J.M. Ferreira Jr., G. Simonelli, J.R. Souza, L.M.N. Góis, L.C.L. Santos, Removal of oil contents and salinity from produced water using microemulsion, J. Water Process Eng. 38 (2020) 101548, https://doi.org/10.1016/j.jwpe.2020.101548.
[4] H.Q. Chang, T. Li, B.C. Liu, R.D. Vidic, M. Elimelech, J.C. Crittenden, Potential and implemented membrane-based technologies for the treatment and reuse of flowback and produced water from shale gas and oil plays: a review, Desalination 455 (2019) 34–57, https://doi.org/10.1016/j.desal.2019.01.001.
[5] M. Coha, G. Farinelli, A. Tiraferri, M. Minella, D. Vione, Advanced oxidation processes in the removal of organic substances from produced water: potential, configurations, and research needs, Chem. Eng. J. 414 (2021) 128668, https://doi.org/10.1016/j.cej.2021.128668.
[6] S. Ghafoori, M. Omar, N. Koutahzadeh, S. Zendehboudi, R.N. Malhas, M. Mohamed, S. Al-Zubaidi, K. Redha, F. Baraki, M. Mehrvar, New advancements, challenges, and future needs on treatment of oilfield produced water: a state-of-the-art review, Sep. Purif. Technol. 289 (2022) 120652, https://doi.org/10.1016/j.seppur.2022.120652.
[7] W.T. Stringfellow, J.K. Domen, M.K. Camarillo, W.L. Sandelin, S. Borglin, Physical, chemical, and biological characteristics of compounds used in hydraulic fracturing, J. Hazard. Mater. 275 (2014) 37–54, https://doi.org/10.1016/j.jhazmat.2014.04.040.
[8] M.A. Al-Ghouti, M.A. Al-Kaabi, M.Y. Ashfaq, D.A. Da'na, Produced water characteristics, treatment and reuse: a review, J. Water Process Eng. 28 (2019) 222–239, https://doi.org/10.1016/j.jwpe.2019.02.001.
[9] B. Liu, B. Chen, B.Y. Zhang, X. Song, G.N. Zeng, K. Lee, Photocatalytic ozonation of offshore produced water by TiO_2 nanotube arrays coupled with UV-LED irradiation, J. Hazard. Mater. 402 (2021) 123456, https://doi.org/10.1016/j.jhazmat.2020.123456.
[10] Y. Yang, X. Zhang, Z. Wang, Oilfield produced water treatment with surface-modified fiber ball media filtration, Water Sci. Technol. 46 (11−12) (2002) 165–170, https://doi.org/10.2166/wst.2002.0733.
[11] K. Elsaid, M. Kamil, E.T. Sayed, M.A. Abdelkareem, T. Wilberforce, A. Olabi, Environmental impact of desalination technologies: a review, Sci. Total Environ. 748 (2020) 141528, https://doi.org/10.1016/j.scitotenv.2020.141528.
[12] R.P. Lively, D.S. Sholl, From water to organics in membrane separations, Nat. Mater. 16 (3) (2017) 276–279, https://doi.org/10.1038/nmat4860.
[13] D.S. Sholl, R.P. Lively, Seven chemical separations to change the world, Nature 532 (7600) (2016) 435–437, https://doi.org/10.1038/532435a.
[14] B. Sapkota, W.T. Liang, A. VahidMohammadi, R. Karnik, A. Noy, M. Wanunu, High permeability sub-nanometre sieve composite MoS_2 membranes, Nat. Commun. 11 (2020) 2747, https://doi.org/10.1038/s41467-020-16577-y.
[15] J. Shen, G.P. Liu, Y. Han, W.Q. Jin, Artificial channels for confined mass transport at the sub-nanometre scale, Nat. Rev. Mater. 6 (4) (2021) 294–312, https://doi.org/10.1038/s41578-020-00268-7.
[16] W.H. Zhang, M.J. Yin, Q. Zhao, C.G. Jin, N.X. Wang, S.L. Ji, C.L. Ritt, M. Elimelech, Q.F. An, Graphene oxide membranes with stable porous structure for ultrafast water transport, Nat. Nanotechnol. 16 (3) (2021) 337–343, https://doi.org/10.1038/s41565-020-00833-9.
[17] S. Wang, S.S. Liang, L. Chen, H.P. Fang, Realizing ultrahigh nanofiltration performance based on small flake reduced graphene oxide membranes, Desalination 528 (2022) 115601, https://doi.org/10.1016/j.desal.2022.115601.
[18] S.X. Zheng, Q.S. Tu, J.J. Urban, S.F. Li, B.X. Mi, Swelling of graphene oxide membranes in aqueous solution: characterization of interlayer spacing and insight into water transport mechanisms, ACS Nano 11 (6) (2017) 6440–6450, https://doi.org/10.1021/acsnano.7b02999.
[19] M.C. Zhang, Y.Y. Mao, G.Z. Liu, G.P. Liu, Y.Q. Fan, W.Q. Jin, Molecular bridges stabilize graphene oxide membranes in water, Angew. Chem. Int. Ed. 59 (4) (2020) 1689–1695, https://doi.org/10.1002/anie.201913010.
[20] L.H. Dai, Z.D. Xiong, W.Y. Xu, K. Qu, Y.X. Wang, S.Y. Gu, H.Y. Cao, Y. Yu, L.F. Lei, S.Y. Li, K. Huang, X.H. Guo, Z. Xu, Two-dimensional confined channels with high-density hydrophilic microregions for enhanced selective water transport, J. Membr. Sci. 671 (2023) 121398, https://doi.org/10.1016/j.memsci.2023.121398.
[21] G.Z. Liu, S. Liu, K. Ma, H.Y. Wang, X.Y. Wang, G.P. Liu, W.Q. Jin, Polyelectrolyte functionalized Ti_2CTx MXene membranes for pervaporation dehydration of isopropanol/water mixtures, Ind. Eng. Chem. Res. 59 (10) (2020) 4732–4741, https://doi.org/10.1021/acs.iecr.9b06881.
[22] Y.X. Liu, Y.S. Sui, A.Q. Dou, L.Y. Wu, Z.H. Tang, X.R. Guo, N. Cao, J.H. Pang, Modulation of the intra-nanopore chemical microenvironment in covalent organic frameworks membranes for efficient water purification and enhanced antifouling

performance, Chem. Eng. J. 529 (2026) 172558, https://doi.org/10.1016/j.cej.2026.172558.
[23] Y.N. Wu, M.M. Jia, S.M. Li, Z. Lu, Y.Y. Wei, H.H. Wang, Positively charged $Ti_3C_2T_X$ membrane for enhanced Li^+/Mg^{2+}sieving, J. Membr. Sci. 717 (2025) 123604, https://doi.org/10.1016/j.memsci.2024.123604.
[24] R.Q. Cao, S.Y. Shi, H.B. Cao, Y.J. Li, F. Duan, Y.P. Li, Surface composite modification of anion exchange membrane by electrodeposition and self-polymerization for improved antifouling performance, Colloids Surf. A Physicochem. Eng. Aspects 648 (2022) 129402, https://doi.org/10.1016/j.colsurfa.2022.129402.
[25] K. Zahri, K.C. Wong, P.S. Goh, A.F. Ismail, Graphene oxide/polysulfone hollow fiber mixed matrix membranes for gas separation, RSC Adv. 6 (92) (2016) 89130–89139, https://doi.org/10.1039/c6ra16820e.
[26] M.C. Zhang, K.C. Guan, Y.F. Ji, G.P. Liu, W.Q. Jin, N.P. Xu, Controllable ion transport by surface-charged graphene oxide membrane, Nat. Commun. 10 (2019) 1253, https://doi.org/10.1038/s41467-019-09286-8.
[27] W.S. Hung, C.H. Tsou, M. De Guzman, Q.F. An, Y.L. Liu, Y.M. Zhang, C.C. Hu, K. R. Lee, J.Y. Lai, Cross-linking with diamine monomers to prepare composite graphene oxide-framework membranes with varying d-spacing, Chem. Mater. 26 (9) (2014) 2983–2990, https://doi.org/10.1021/cm5007873.
[28] S.J. Xia, M. Ni, T.R. Zhu, Y. Zhao, N.N. Li, Ultrathin graphene oxide nanosheet membranes with various d-spacing assembled using the pressure-assisted filtration method for removing natural organic matter, Desalination 371 (2015) 78–87, https://doi.org/10.1016/j.desal.2015.06.005.
[29] G. Foli, A. Kovtun, F. Liscio, E. Battaglini, S. Ligi, M. Fiorini, M. Minelli, V. Palermo, Tuneable permeability to H_2, CO_2, He, and Ar in graphene oxide-PDDA self-assembled multilayers, yielding good selectivity at high flux, Adv. Mater. Interfaces 11 (2024) 2300357, https://doi.org/10.1002/admi.202300357.
[30] K.H. Thebo, X.T. Qian, Q. Zhang, L. Chen, H.M. Cheng, W.C. Ren, Highly stable graphene-oxide-based membranes with superior permeability, Nat. Commun. 9 (2018) 1486, https://doi.org/10.1038/s41467-018-03919-0.
[31] Y.L. Qian, X.L. Zhang, C.Y. Liu, C. Zhou, A.S. Huang, Tuning interlayer spacing of graphene oxide membranes with enhanced desalination performance, Desalination 460 (2019) 56–63, https://doi.org/10.1016/j.desal.2019.03.009.
[32] S.F. Wang, L.X. Yang, G.W. He, B.B. Shi, Y.F. Li, H. Wu, R.N. Zhang, S. Nunes, Z. Y. Jiang, Two-dimensional nanochannel membranes for molecular and ionic separations, Chem. Soc. Rev. 49 (4) (2020) 1071–1089, https://doi.org/10.1039/c9cs00751b.